Spatio-temporal Variation of Bright Ephemeral Features on Titan's North Pole

Rajani Dhingra, Jason Barnes, Michael Heslar, Robert Brown, Bonnie Buratti, Christophe Sotin, Jason Soderblom, Sebastien Rodriguez, Stéphane Le Mouélic, Philip Nicholson, et al.

The Planetary Science Journal, 1:31 (11pp), 2020 September https://doi.org/10.3847/PSJ/ab9c2b

Spatio-temporal Variation of Bright Ephemeral Features on Titan's North Pole

Rajani D. Dhingra[1,2], Jason W. Barnes[2], Michael F. Heslar[2], Robert H. Brown[3], Bonnie J. Buratti[1], Christophe Sotin[1], Jason M. Soderblom[4], Sebastien Rodriguez[5], Stéphane Le Mouélic[6], Philip D. Nicholson[7], Kevin H. Baines[8], Roger N. Clark[9], and Ralf Jaumann[10]
[1] Jet Propulsion Laboratory, Caltech, Pasadena, CA, USA; rhapsodyraj@gmail.com, rajani.dhingra@jpl.nasa.gov
[2] Department of Physics, University of Idaho, Moscow, ID, USA
[3] Department of Planetary Sciences, University of Arizona, Tucson, AZ, USA
[4] Department of Earth, Atmospheric and Planetary Sciences, MIT, Cambridge, MA, USA
[5] Université de Paris, Institut de physique du globe de Paris, CNRS, F-75005 Paris, France
[6] Laboratoire de Planetologie et Geodynamique, CNRS UMR6112, Universite de Nantes, France
[7] Cornell University, Astronomy Department, Ithaca, NY, USA
[8] Space Science & Engineering Center, University of Wisconsin-Madison, Madison, WI, USA
[9] Planetary Science Institute, Tucson, AZ 85719, USA
[10] Deutsches Zentrum für Luft- und Raumfahrt, D-12489, Germany
Received 2019 December 9; revised 2020 June 1; accepted 2020 June 2; published 2020 July 28

Abstract

We identify and document the instances of bright ephemeral features (BEF)—bright areas that appear, disappear, and shift from flyby to flyby on Titan's north pole, using the Cassini Visual and Infrared Mapping Spectrometer data set, thereby developing a sense of their spatial distribution and temporal frequency. We find that BEFs have differing geographic location and spatial extents. However, they have similar observation geometries and orders of surface area coverage and are mostly accompanied by specular reflections. We find the BEFs to represent either broad specular reflection off of a recently wetted surface on the north pole of Titan or a near-surface fog—both owing to probable recent rainfalls. Our surface model constrains the surface roughness to be of 9°–15° indicating the approximate vertical relief of the region to be that of cobbles. We also find that within less than two Titan days the BEF (if on the surface) might infiltrate into the subsurface. We hypothesize the parts of BEFs that extend into the maria to be precipitation fog.

Unified Astronomy Thesaurus concepts: Saturnian satellites (1427)

1. Introduction

Detection of surface changes on Titan have been difficult owing to its complex and thick atmosphere (Kuiper 1944). The absorption and scattering by atmospheric gases and aerosols (Tomasko & Smith 1982) and the non-Lambertian surface phase functions (Solomonidou et al. 2014) make it difficult to hash out the surface signal from that of the atmosphere. Definitive surface changes could be credited to rainfall events on Titan's surface but have been observed otherwise too (MacKenzie et al. 2019; Heslar et al. 2020). Of the rainfall events documented, one happens to be at the south pole of Titan over the Arrakis Planitia (Turtle et al. 2009). Another detected surface change later attributed to giant cloudbursts was found at the equatorial region (Turtle et al. 2011; Barnes et al. 2013a). Both of these observations were detected by Imaging Science Subsystem (ISS) but the equatorial observation was later followed by Visual and Infrared Mapping Spectrometer (VIMS) as well. Dhingra et al. (2019) discuss the surface changes observed over Titan's north pole hypothesized as either a wet sidewalk (WSW) feature indicating a recently rainfall wetted surface that reflects brightly at 5 μm or on a near-surface fog.

Cloud coverage (Griffith et al. 2009; Rodriguez et al. 2009, 2011; Turtle et al. 2009, 2011, 2018; Brown et al. 2010; le Mouélic et al. 2018) and surface rain were both first observed at the south pole, when Cassini arrived during southern summer, and then later in the equatorial region. These observations were broadly consistent with the global circulation models (Tokano & Neubauer 2005; Rannou et al. 2006; Mitchell et al. 2006; Tokano 2011; Lora & Mitchell 2015; Mitchell & Lora 2016). The circulation models also predicted increasing cloud and rain activity at the north pole as north polar summer approached.

VIMS and ISS finally observed the onset of cloud activity on the north pole of Titan (Turtle et al. 2018). Moreover VIMS also observed bright ephemeral features (BEFs) on the north pole of Titan in the T120 flyby (2016 June 7). Dhingra et al. (2019) attribute the observation in the T120 flyby to broad specular reflection off of a wetted land surface. When a rough surface gets wetted by rainfall, liquid methane drapes over the crests and troughs forming a thin surface layer (Figure 1). This liquid layer smooths out the surface at small scales that are comparable to the VIMS wavelengths (1–5 μm) and hence are observed as a broadly specularly reflecting layer that is away from the specular point. When viewed far from a specular geometry, a wet surface would appear darker than a dry surface (Figure 1), as seen by ISS in previous wetting events (Turtle et al. 2009, 2011). But when viewed somewhat near a specular observation geometry, the area would reflect brightly.

Motivated by the T120 observation (Dhingra et al. 2019), we sift through other VIMS north polar observations to detect more transient features. We find additional transient features—bright areas that appear, disappear, and shift from flyby to flyby (Figure 2). In this study, we document the temporal and spatial evolution of these bright areas that we termed BEFs in our discovery paper.

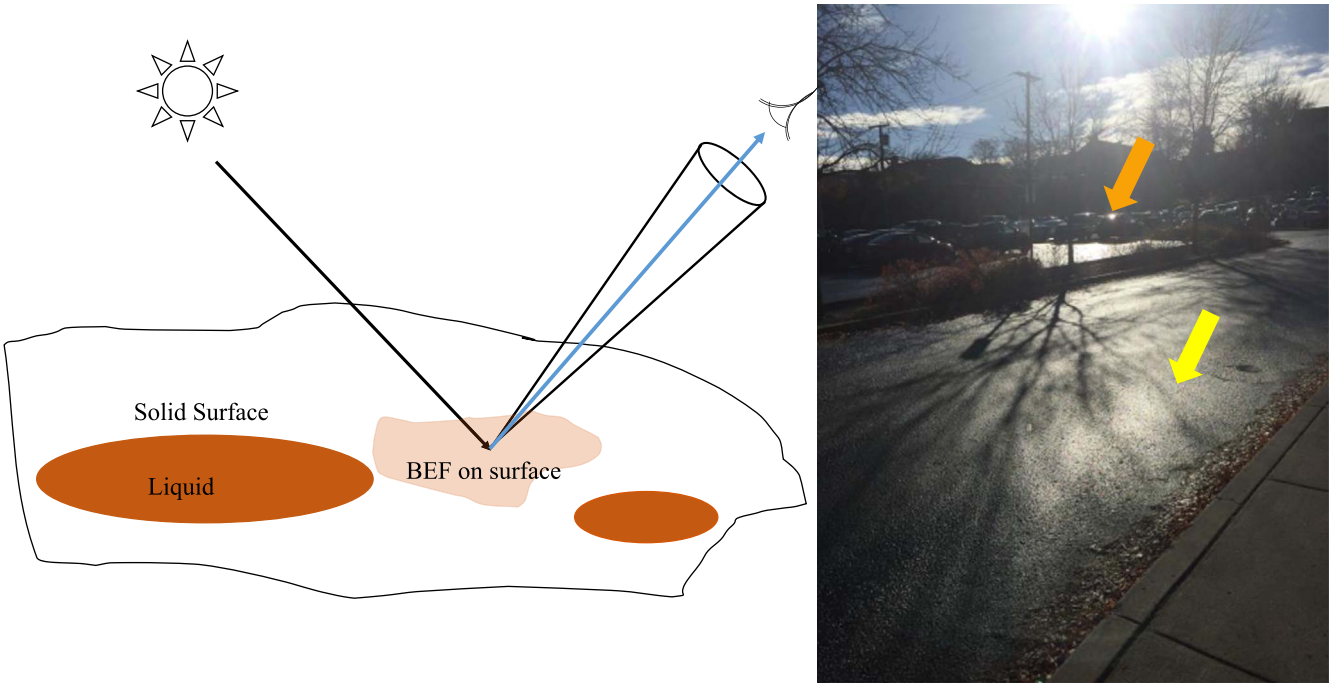

Figure 1. We show (in the left) a cartoon to explain the origin of the BEF. The orange ovals are lakes on Titan while the transparent orangish feature is a recently wetted region. The blue arrow indicates the geometry for direct specular reflection where incidence and emission angles are equal. The cone shows the light reflected within a small angle of the perfect reflection. The intensity of the reflection tails off outside of the cone. On right we show a WSW effect on a bright morning after rainfall at the University of Idaho parking lot. The specular reflection (orange arrow) arises out of the rear windshield of the car. The other regions at the right geometries are reflecting brightly (yellow arrow) or look darker. The south polar darkening that Turtle et al. (2009) documented would be in a geometry like the darker region in this WSW picture. The figure's change contrast in the subsequent images due to the various platforms of the analysis.

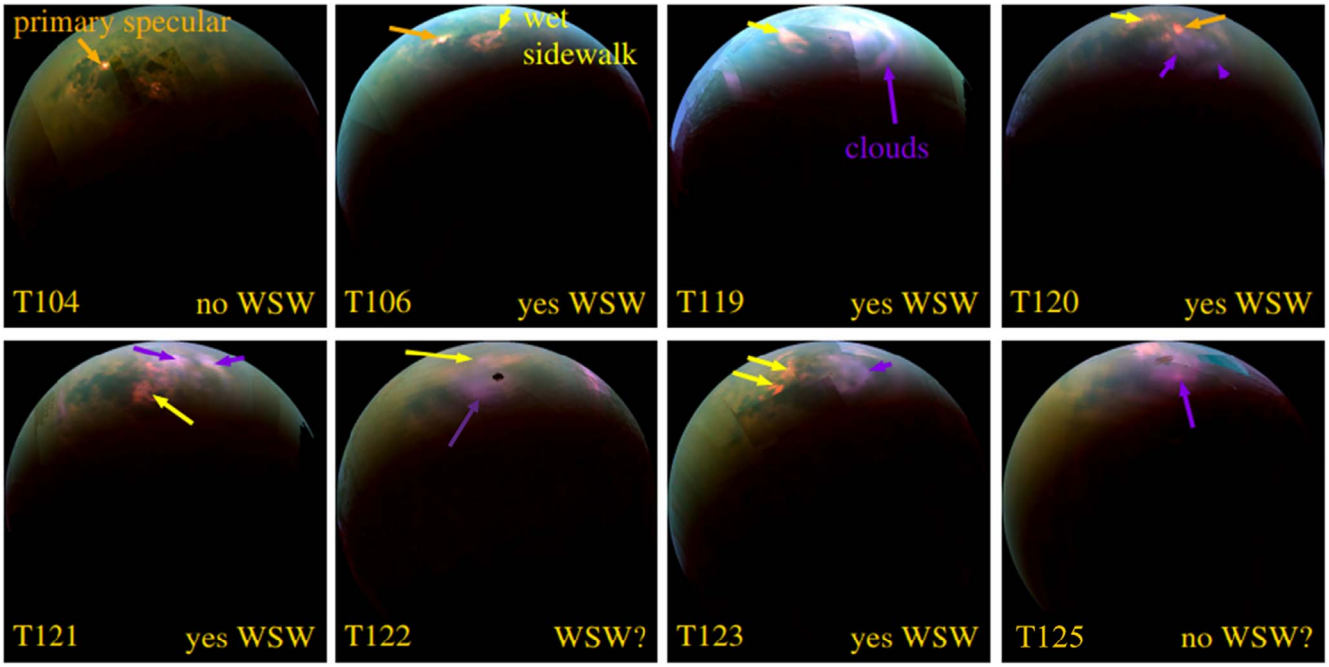

Figure 2. We show here orthographic projections of VIMS mosaics from eight different Cassini Titan flybys centered on 23°–40°N, 180°E. The color scheme brings out specular features in orange and clouds in purple (red is mapped to 5 μm, green to 2 μm, and blue to 2.73 μm). The orange arrows show the specular reflection in each flyby. The purple arrows show the cloud cover over the north pole of Titan. The BEFs are shown by yellow arrows.

Only a few rainfall observations have been documented in the 13 years of the Cassini mission. The low frequency of Titan's encounters (~1 flyby per month), the rapid evaporation rate (~30 m/Titan year, from Mitri et al. 2007), and the fact that only a small number of atmospheric windows are able to probe the surface (Sotin et al. 2005) make the observation of a BEF challenging. Moreover the polar regions of Titan, where BEF occur, are only illuminated during a fraction of the mission duration.

Observation geometry, position of the spacecraft, evaporation rate, and atmospheric scattering augment the difficulty of observing rainfalls on Titan. The significance of this

Table 1
We Show here Parameters for the VIMS Observations on Various Flybys that Show Indications of the WSW Effect

Flyby	Date	Phase (deg)	Cube Used	Exp Time (ms)	*i (deg)*	*e* (deg)	Pixel Res (km pixel^{-1})
T106	2014 Oct 24	120	CM_1792827895_1	160	71	49	37
T119	2016 May 6	125	CM_1841258035_1	160	63	68	24
T120	2016 Jun 7	116	CM_1844022476_1	160	51	64	48
T121	2016 Jul 25	113	CM_1848148220_1	160	63	51	32
T123	2016 Sep 27	112	CM_1853659871_1	180	53	60	38

Note. The best cubes are those acquired near Titan, thereby achieving the finest-scale resolution. The incidence angle *(i)* and emission angle *(e)* shown are typical for the BEF on that particular flyby.

documentation is that we might be able to determine when and where has it rained on the north pole of Titan without having to actually observe the rainfall event.

Our study is driven by finding the answer to the question, "when and where does it rain on Titan?" The answer to which will help in the determination of the global methane transport and global liquid distribution. Cloud observations help us determine the probability of rainfall and confirm if local environmental conditions (e.g., convective and saturated air) are favorable for rain. However, figuring out the location and time of the rainfall is important to solve the puzzle of the asymmetric liquid distribution on Titan.

In Section 2, we enlist the data used and the observations of the BEF in other flybys apart from T120. Section 3 entails each observation in detail such that the geographic location and area covered. We calculate the surface roughness of the BEFs in Section 4.1. In Section 4.2, we discuss an approximation of the amount of rainfall constrained by evaporation and infiltration rates. In Section 5, we discuss the possibility of BEFs being fog, which is followed by Section 6 with a discussion, conclusions, and details of future work.

2. Data

We calibrate the Planetary Data System (PDS) data using the algorithm described by Barnes et al. (2007a), except that we turn the despike off. Each cube is despiked by hand as the automated despiker cleans the data of primary specular glints in such a way that degrades its overall utility in a specular context. We also use the ISS (https://planetarymaps.usgs.gov/mosaic/Titan_ISS_P19658_Mosaic_Global_4km.tif) north polar map to look at the observation in spatial context to manually draw the contours of the BEF using ArcGIS.

Table 1 documents the data used in this study, the flyby, the cube used for the analysis, and the observation geometry. We basically sift through all the flybys after the T100s (2014 April) and use the cubes from the flybys where we see a BEF in our WSW color composite ($R = 5\,\mu$m averaged over channels 336–351, $G = 2\,\mu$m channel 165, and $B = 2.73\,\mu$m channel 208, Figure 2).

3. Details of Each Observation

In addition to the discovery instance of T120 observation, we now recognize additional observations that show the BEF on the north pole of Titan. In this section we identify and map each instance of BEF.

3.1. T106

Our discovery observation of the BEF in the T120 flyby (Figure 3) happened on 2016 June 7. It motivated us to look for the same region covered in previous flybys. The T120 BEF region had been last seen in T106 flyby. While we confirmed that the bright region in T120 was indeed ephemeral owing to its absence in T106, we found another BEF in the T106 flyby itself. We devised the WSW color composite (Figure 3(a)) because this helped us in hashing out the clouds in purplish hues, while pinkish features are closer to the surface or near-surface. Figure 3(b) shows the ISS map in polar projection and the spatial extent of the T120 BEF marked in magenta.

Flybys before the T106 do not show any observable BEFs. The T106 flyby happened on 2014 October 24 and began the series of several directed north polar flybys and BEF observations. As shown by a yellow arrow in Figure 4(a), the BEF partly covers the land between Punga Mare and Ligeia Mare and extends into Ligeia Mare. The extention into Ligeia Mare is a surprising observation and complicates our analysis about the BEF's location vertically, i.e., if it is right on the surface or up in the atmosphere. It is also a possibility that the BEF is an amalgamation of two different vertical features—a near surface (over the Mare) and on the surface (WSW)—seemingly appearing as one feature. The adjacent Figure 4(b) shows the outline of the extent of the BEF in green. We show T120's outline (in magenta) indicating that the BEF's geographic location has changed.

The areal coverage of T106 BEF totals $\sim$115,000 km^2 over the latitudes from 90°N to 80°N and longitudes of 210°W to 300°W. The T106 flyby also has a direct specular reflection on the eastern edge of Kraken Mare over Gabes Sinus. The latitude and longitude of the inferred specular point are 70°.7N, 293°W. The great circle distance from the specular point is $\sim$715 km, indicating that the BEF is close enough to the specular point (or in the specular cone as shown in Figure 1).

We devise a triple peak color composite ($R = 2.7\,\mu$m, $G = 2.8\,\mu$m, and $B = 2.9\,\mu$m) to better separate the different portions of a BEF (Figure 4(c)). The 2.7–2.8 μm sub-window (McCord et al. 2006) in Titan spectra looks at the surface. We have the longest optical paths through Titan's atmosphere when we look through an atmospheric window (2.7–2.8 μm in this case; Barnes et al. 2007a, 2007b, 2013b; McCord et al. 2008) and hence have maximum sensitivity to the surface. As we move away from the band center and look at the wings of an atmospheric window, we are looking through more atmosphere (higher optical depth) while moving away from the surface, at some altitude. The wing of the sub-window lies at 2.9 μm moving away from the surface. Since we assign the 2.9 μm window to blue, any whitish feature is probably in the atmosphere. Similarly we assign the 2.8 μm to green so the greenish feature is on the surface or closer to the surface. Motivated by the extensions of BEFs into Titan's maria, this color composite helps us in ruling out if the other

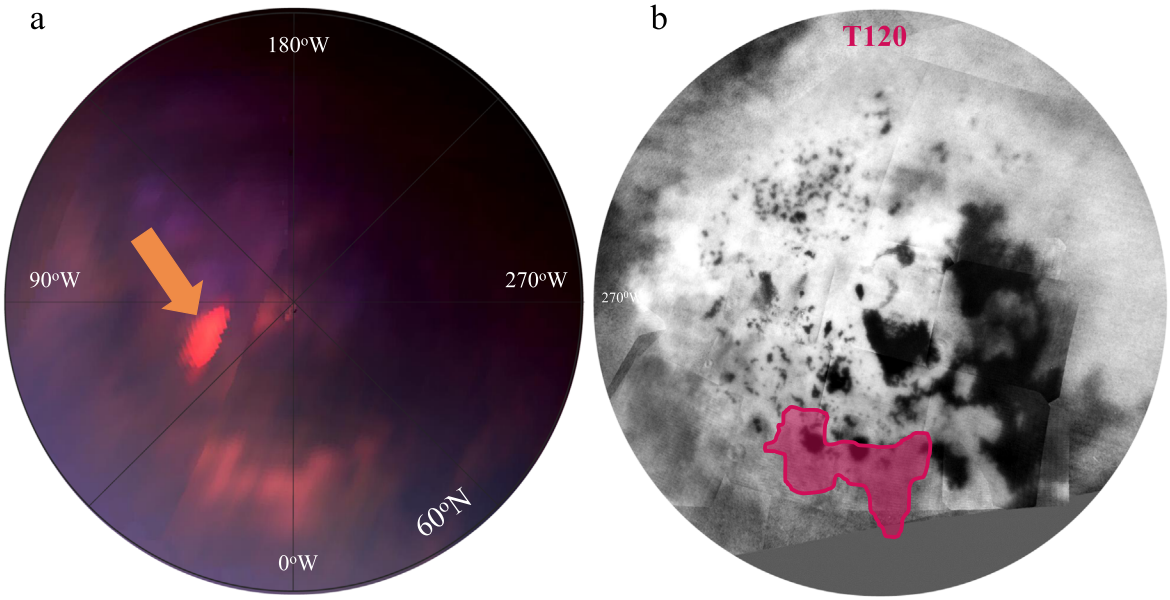

Figure 3. Panel (a) shows a polar stereographic projection of T120 flyby in VIMS WSW color composite (red is mapped to 5 μm, green to 2 μm, and blue to 2.73 μm). The orange arrow marks the location of direct specular reflection. Panel (b) shows the extent of T120 WSW marked in magenta over a base map of ISS. The other magenta feature at the north pole is another WSW feature. The subsequent figures differ in contrast due to the various platforms of analysis.

portions of the BEF are indeed on the surface or at some height above the surface. Different parts of the BEF show up in different hues of white or green in every flyby based upon the color scheme.

The feature at the north pole (near Punga) looks whitish indicating the atmospheric location of the BEF. The extension of the BEF into Ligeia Mare looks greenish indicating the surface location of the feature (Figure 4(d)).

3.2. T119

T119 (2016 May) was the preceding observation to our T120 (2016 June) discovery observation. We see a BEF in the T119 flyby yet not at the location where T120 BEF (magenta) was. The spatial extent covers an area of ~70,000 km^2 over the approximate latitudes of 81°N–68°N and longitudes of 66°E–17°E. The T119 flyby has no specular observation as the predicted specular point does not move over liquid bodies.

The T119 BEF observation overlays the land between Jingpo Lacus and Kraken Mare as shown in Figure 5(a) in the VIMS color composite. Figure 5(b) marks the spatial extent of the BEF in red. Although the core of this feature overlays land surface, a thin portion juts into Kraken Mare.

We use the triple peak color scheme on T119 (Figures 5(c) and (d)) and observe that the laminar extension of T119 BEF and the portion of the BEF that overlays Jingpo Lacus look different than the core of the feature. The laminar extension of T119 BEF is not even perceivable in the triple peak color scheme. This certainly helps the case of the BEF being a wetted surface; the laminar could be a thin cloud/fog that is near Kraken's surface, as may also result from a recent rain event.

However, the imperceptibility of the laminar extension could also just be because a fog over a dark sea is harder to see than a fog over a brighter surface. It is also possible that the fog changes altitude as it move between land and sea and thus appears different from orbit.

3.3. T121

T121 (2016 July) is one of the most cloud-heavy flybys of the north pole and probably the whole Cassini mission. The north pole is almost totally under cloud cover in our WSW color composite (see Figure 6(a)) except the bright BEF peeking through the clouds and the southern Kraken Mare.

The T121 flyby also has a specular reflection that arises from the geographical location 83°N and 6°4W. The specular reflection arises from land (southwest of Punga coast). The fact that the specular reflection arises from land surface close to the Punga coastline might indicate that either it is a wetted surface or a marshy land near the coastline. However, there are several small lakes observed in the ISS observation in the vicinity of the specular reflection and it is quite likely that the glint is coming from one of those lakes. The great circle distance of the center of the core of the BEF feature from the specular point is ~400 km.

The BEF overlays the land between Ligeia Mare, Punga Mare, and Kraken Mare (Figure 6(b)). There is a finger-like feature poking into Ligeia Mare that we call the "Ligeia finger" in the rest of this work that is different from the Radio Detection and Ranging (Radar) observations of the magic island (Hofgartner et al. 2016).The Ligeia finger very prominently stands out in the orthographic images of the north pole, making us question if the location of the "Ligeia finger" or all of the BEF is indeed on the surface. The feature could as well be a near-surface feature.

Our triple peak color scheme ($R = 2.7$ μm, $G = 2.8$ μm, and $B = 2.9$ μm) shows the Ligeia finger along with some portion of the BEF in a bluish-white hue as compared to the otherwise greenish hue of the core BEF (Figures 6(c) and (d)). This could mean that some regions of the BEF, including the "Ligeia finger" extension of the BEF, are probably located at a different height in the atmosphere. This triple peak analysis indicates that the height of the Ligeia finger is different from that of the BEF. The finger also has a dark gap in a triple peak image, which may suggest that it is distinct from the BEF.

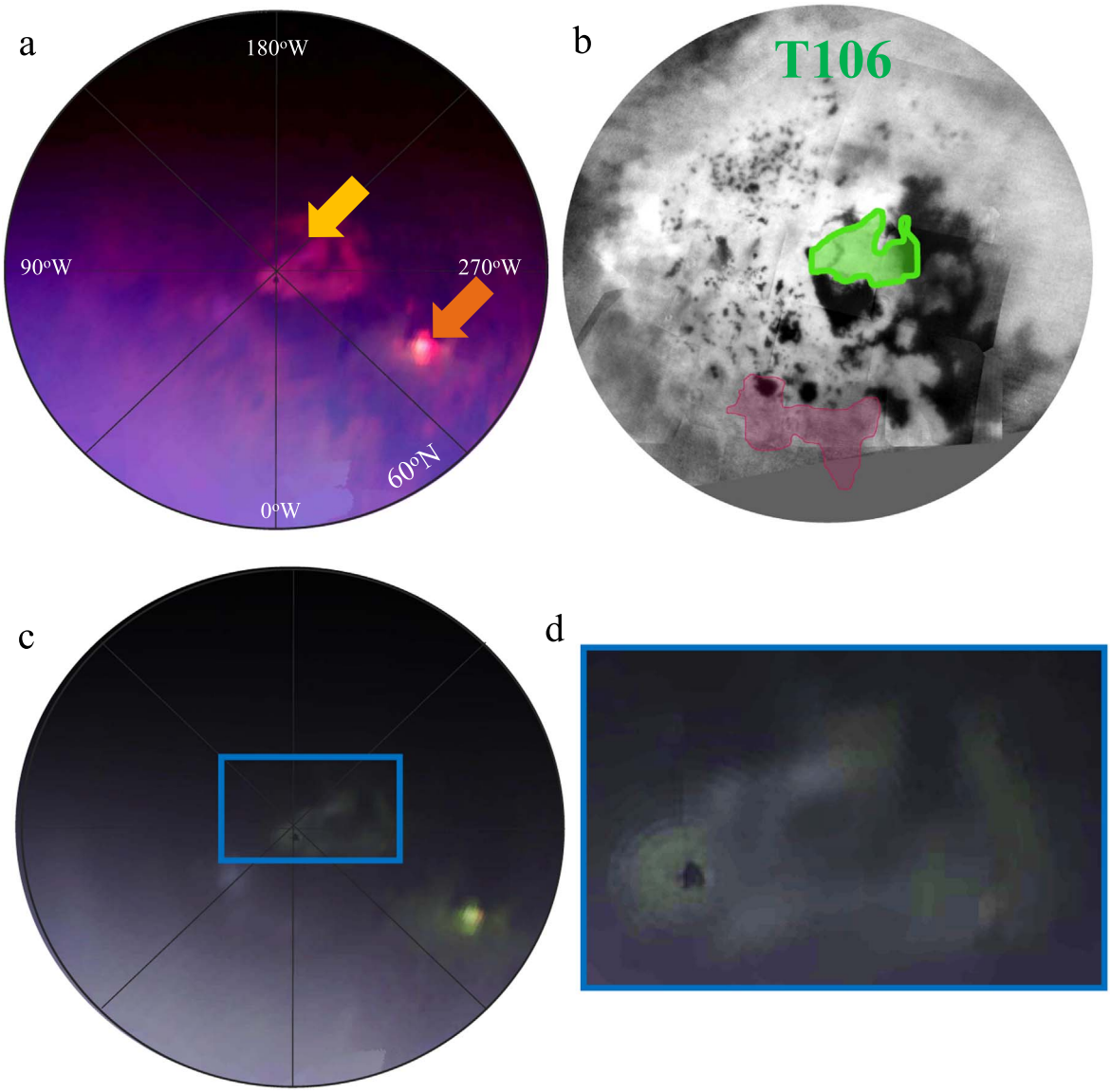

Figure 4. Panel (a) shows the polar stereographic projection of T106 flyby in VIMS WSW color composite. The orange arrow marks the location of direct specular reflection. Panel (b) shows the extent of the T106 BEF in green on the base map of Radar and ISS. Faded magenta outline marks the T120 BEF extent indicating that the feature is at other geographical locations of the north pole. Panel (c) shows the T106 flyby in the VIMS triple peak color ($R = 2.69$ μm averaged over channels 205–207, $G = 2.77$ μm channels 210–212, and $B = 2.90$ μm channels 218–219) composite. Panel (d) is the zoomed-in and cropped BEF in a triple peak color scheme. Features at surface look greenish while clouds look whitish blue.

3.4. T123

The T123 flyby that occurred on 2016 September (the same year as all the other flybys that display BEFs, except T106) is our last flyby where we see the BEF before the Cassini mission ended.

However, we can clearly distinguish the BEF in this flyby by the lower spatial sampling (Figure 7(a)). The BEF overlays the land between Jingpo Lacus and Bolsena Lacus and covers an area of $\sim$120,000 km^2 (Figure 7(b)). A portion of the BEF overlays Jingpo Lacus but since this flyby is of a lesser spatial sampling we do not run the triple color scheme on this observation. Another thing to note is the spatial extent of the T123 BEF overlaps that of T120's and T119's partly. The approximate inferred specular point of this flyby is 69°.56N and 33°.36E that overlays the land surface off the eastern coast of southern Kraken Mare. We do observe a direct specular reflection from the land near the shores of Kraken Mare that again indicates an ephemeral puddle, wetted land surface, marshy shorelines, or a specular glint near the shore of Kraken just as the waves hit the shoreline. Only a pixel-by-pixel analysis of all the cube acquired during this flyby can assess the location and the nature of the specular point.

3.5. Null Detections

In between our first BEF detection in the T106 flyby and the next one in the T119 flyby, there are no north polar Cassini data of Titan acquired. The later north polar observations of Titan (T124, T125, and T126) do show a plethora of cloud cover yet not a BEF. The next flyby, T124, has a specular reflection but no BEF whereas T125 has a probable BEF signature but because of very low spatial sampling, we do not include the T125 observation in our work here. T126, the final VIMS close flyby of Titan, has no detected BEF.

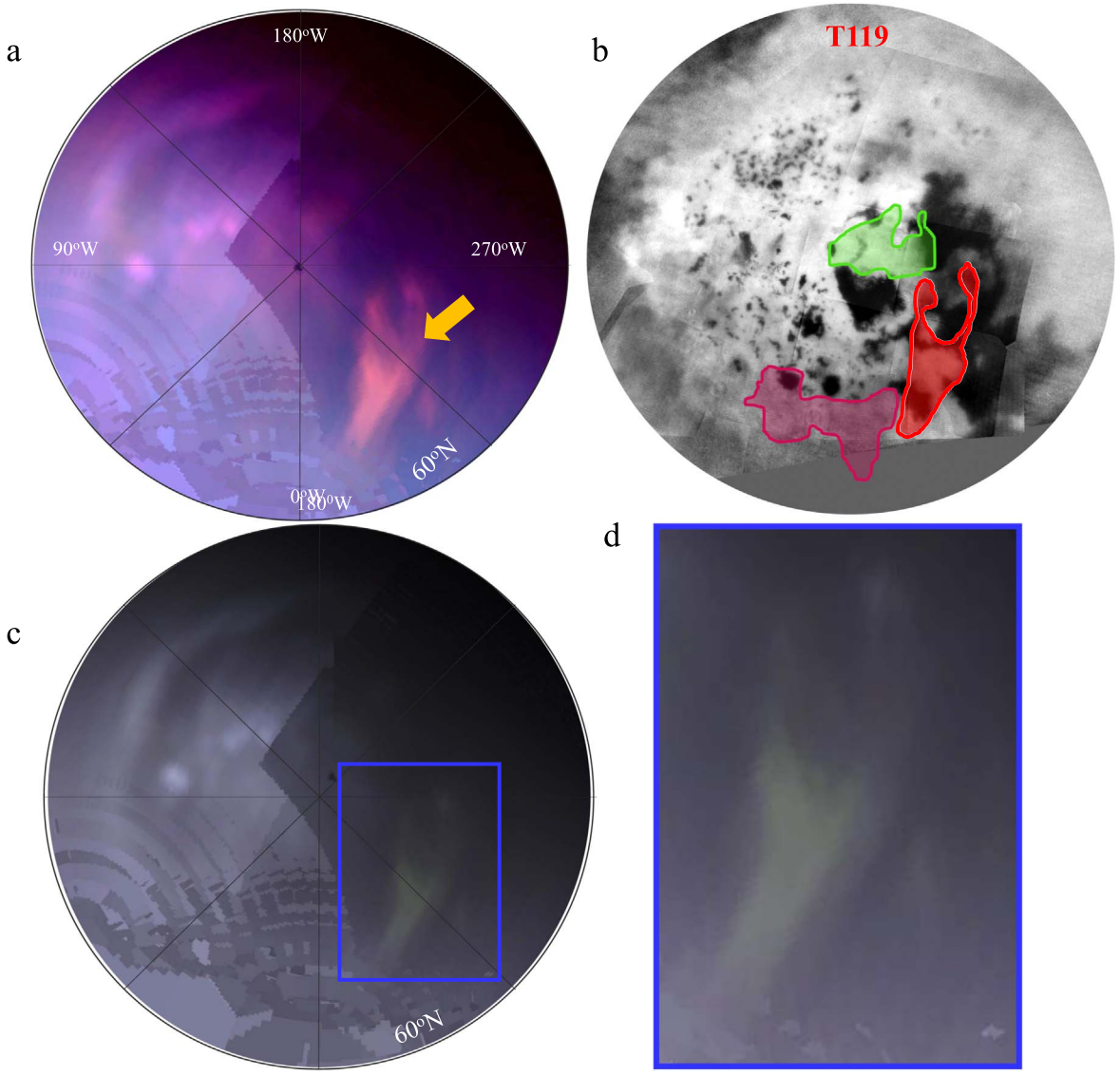

Figure 5. Panel (a) shows the polar stereographic projection of the T119 flyby in VIMS WSW color composite. Panel (b) shows the extent of the T119 BEF in red on the base map of ISS. Faded magenta and green outlines mark the T120 and T106 BEF extent indicating that the feature is at other geographical locations of the north pole. Panel (c) shows the T119 flyby in the VIMS triple peak color ($R = 2.7$ μm, $G = 2.8$ μm, and $B = 2.9$ μm) composite. Panel (d) is the zoomed-in and cropped BEF in a triple peak color scheme. Features at surface look greenish while clouds look whitish blue (see the text for details).

4. WSW Scenario

When some of the BEFs are surface features, we can derive the surface roughness by using the observation geometry constraints of a broad specular reflection where the facets are tilted such that the reflection is toward the observer (Cassini). We derive the surface-roughness constraints followed by placing rough restraints on the rainfall volume in the below subsections.

4.1. Surface-roughness Constraints

We use a numerical planetary specular model (Soderblom et al. 2012; Barnes et al. 2014) with Gaussian-distributed slopes and azimuthal symmetry for the same observation geometry as our BEF observations to understand the surface roughness. This analysis also helps in cataloging the (model-derived) surface roughnesses for the north pole for the surface-roughness values.

We observe that the surface-roughness values vary between 9° and 15° (Table 2). We use the observational and theoretical constraints to derive the length scales over which the model-determined surface roughness occurs.

Surface tension restricts the spread of liquid methane rain over an icy bedrock (17 dyne cm^{-1}; Sprow & Prausnitz 1966); water surface tension is 70 dyne cm^{-1} (Vargaftik et al. 1983). Liquid methane spreads readily as it has a lower surface tension than water. Radar data provide an observational constraint, suggesting the topography of the region to be rough and variegated at the Radar wavelength scale (∼2 cm). All the flybys discussed in this work are on the north pole. We see that the BEF regions usually overlap the Synthetic Aperture Radar (SAR)-bright, dark dissected uplands and darker, lower plains that usually have a high local slope (Birch et al. 2017).

To infer the topography of the BEF regions under these constraints, we assume different grain size dimensions, namely gravel (2–64 mm), cobble (64–256 mm), and boulder (200–630 mm) as length scales and calculate the corresponding

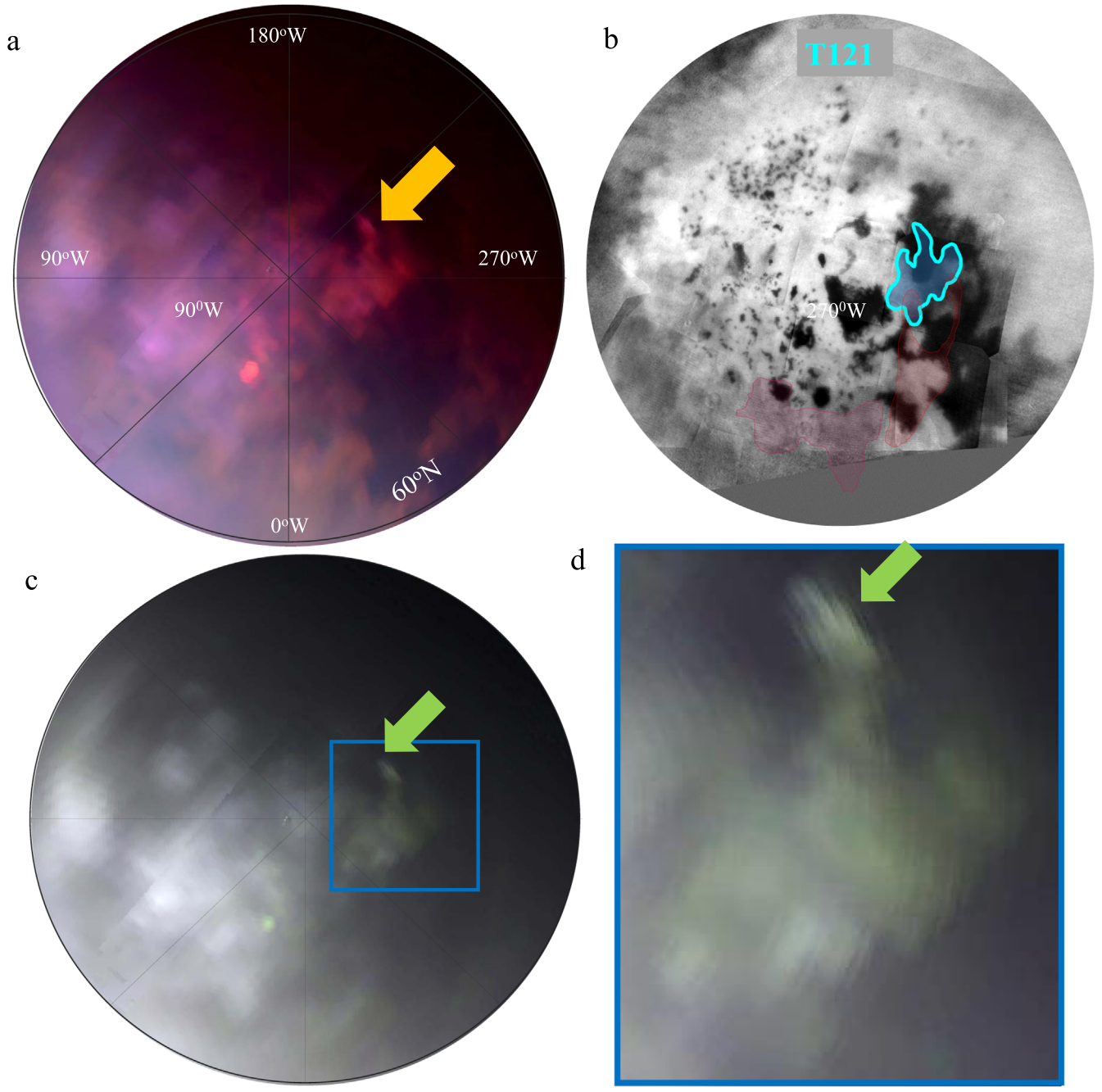

Figure 6. Panel (a) shows the polar stereographic projection of the T121 flyby in VIMS WSW color composite. Panel (b) shows the extent of the T121 BEF in cyan green on the base map of Radar and ISS. Faded magenta, green, and red outlines mark the T120, T106, and T121 BEF extent indicating that the feature is at other geographical locations of the north pole. Panel (c) shows the T121 flyby in the VIMS triple peak color composite. Ligiea Finger is indicated by a green arrow in the figure panels (c)and (d). Panel (d) is the zoomed-in and cropped BEF in a triple peak color scheme. Features at surface look greenish while clouds look whitish blue.

vertical relief. If the primary source of our measured ∼9°–15° surface roughness were gravel, then under the surface-roughness conditions, the vertical relief would range from submm to a couple of millimeters (0.7–21 mm). If cobbles instead cause the observed roughness, then the peak to trough surface heights are ∼21–85 mm. The range (∼8.5 cm) for the values of cobbles is larger than the observational constraint from the Radar data. We therefore infer that the geomorphology of the region corresponding to the BEF could be a mix of gravels and small cobbles of vertical relief ranging from submm to a couple of centimeters that very much sounds like the Huygen's landing site (Soderblom et al. 2007).

4.2. Rain Quantity

We try to place constraints on the quantity of rain delivered to the surface using a simple mass-balance model (Dhingra et al. 2018). Given that the WSWs do not occur in the same place from flyby to flyby, we use their limited longevity along with models of evaporation (Mitri et al. 2007) and infiltration with hydraulic conductivity (Hayes et al. 2008; Horvath et al. 2016) to derive limits on the minimum quantity of liquid that could have produced each observed feature.

The longevity of the rainfall is derived by the time spans between the two flybys. There are no prior observations for T106 and T119 flybys. However, T120, T121, and T123 flybys

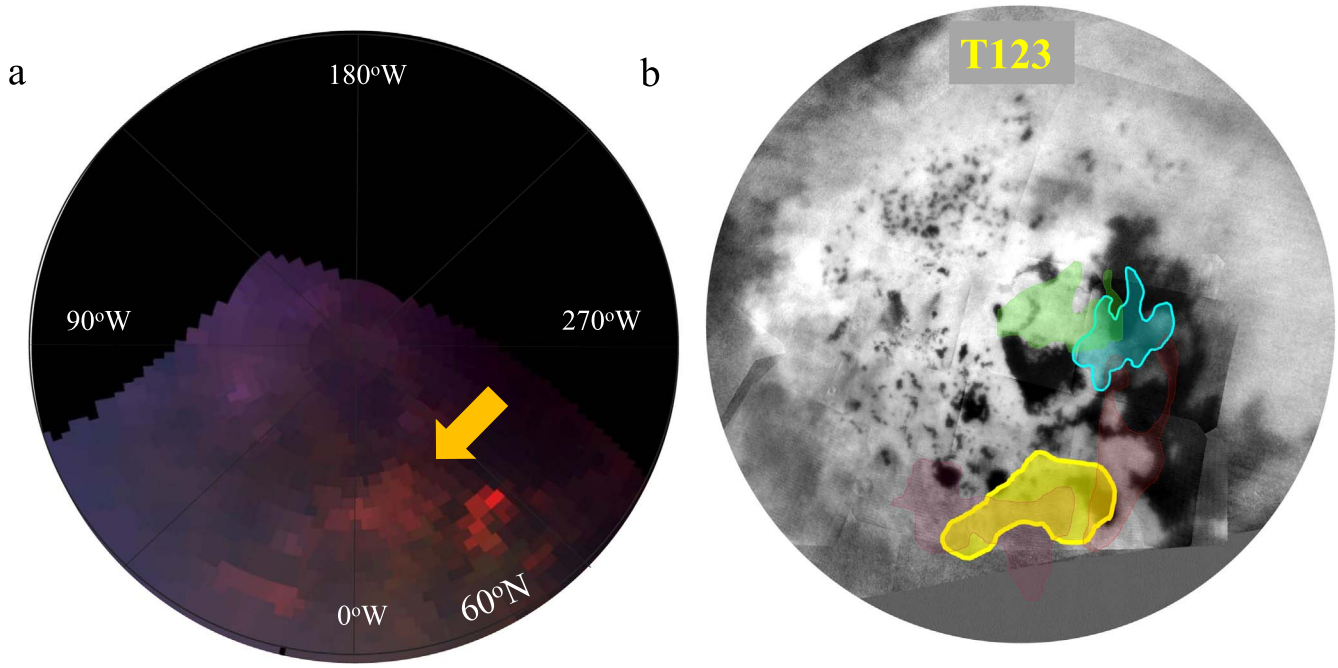

Figure 7. Panel (a) shows a polar stereographic projection of T123 flyby in VIMS WSW color composite (red is mapped to 5 μm, green to 2 μm, and blue to 2.73 μm). Panel (b) shows the extent of T123 WSW marked in yellow over a base map of Radar and ISS.

Table 2
We Tabulate the Model-derived Surface-Roughness Values here for Each Flyby BEF Observed

Flyby	Cube Used	Sp. Pt. Location	Dist. from Sp. Pt. (km)	Surface Roughness (deg)
T106	CM_1792827895_1	Sea (Kraken)	715	9
T119	CM_1841258035_1	NA	NA	NA
T120	CM_1844022476_1	Lake (Xolotlan)	632	10–15
T121	CM_1848148220_1	Land (southwest of Punga coast)	424	NA
T123	CM_1853659871_1	Land (Kraken coast)	452	9–10

Note. "NA" in the columns indicate either there was no specular reflection observed to model surface roughness or the model fails to generate a specular reflection that arises from a land surface.

do have prior flybys to determine their longevities. Table 1 shows that T120 was observed two Titan days after T119 indicating a longevity of maximum two Titan days. Similarly, T121 was observed three Titan days later, and T123 was observed four Titan days later. We use the evaporation rate of 30 m/Titan year (Mitri et al. 2007) and infiltration with hydraulic conductivity using the percolation velocity of liquid methane for Titan conditions as assumed in Horvath et al. (2016). The mass-balance model for this calculation we consider is as given below. Here, V is the volume of the rainfall, P is the precipitation rate, E is the evaporation rate, A_c is the catchment area, $A_{\rm BEF}$ is the area of the BEF, and $K_{\rm hy}$ is the hydraulic conductivity as described in Equation (3):

$$\frac{dV}{dt} = (P * A_c - (E + K_{\rm hy}) * A_{\rm BEF}). \quad (1)$$

We assume a linear decrease in volume and that $A_c = A_{\rm BEF}$ (owing to the less solid surface area available on Titan's north pole):

$$\Delta V = [P * A_{\rm BEF} - (E + K_{\rm hy}) * A_{\rm BEF}]^*\Delta t, \quad (2)$$

where ΔV is the change in volume, $A_{\rm BEF}$ is the area of the BEF, E is the evaporation rate, Δt is the longevity of the BEF and $K_{\rm hy}$, and the hydraulic conductivity is expressed as

$$K_{\rm hy} = \frac{k\rho g}{\mu}. \quad (3)$$

Here, κ is the percolation velocity that we use from Horvath et al. (2016) for low and high permeabilities, ρ is the density of methane, μ is the viscosity of methane, and g is Titan's gravity.

Our calculations shown in Table 3 indicate that the change in volume of rainfall is a negative quantity for the observed longevity if the BEFs behave like a WSW (Figure 1). This suggests that if the BEFs are WSW on the surface they must be very fresh and less than a few hours old. Rainfall would not be observable after a whole span of two/three/four Titan days and might infiltrate or evaporate before our next observation. However, we wish to note that this calculation disagrees the precipitation induced brightening Barnes et al. (2013a) observed in the equatorial region of Titan, where after the cloudburst the areas darken for months, then brighten for a year before reverting to their original spectrum. In fact, the cold temperatures near the pole must perhaps freeze the methane rain into methane or ethane ice that would melt more slowly there (Steckloff et al. 2020).

Table 3
We Tabulate the Values We Derive Using Our Mass-balance Model to Approximate the Quantity of Rainfall

Flyby	A_{BEF}(~km ^{2})	Longevity (Titan Days)	Change in Volume
T106	115,000	Unknown	Unknown
T119	70,273	2	All percolated/evaporated
T120	120,000	3	All percolated/evaporated
T121	120,386	4	All percolated/evaporated
T123	119,340	At least 2	All percolated/evaporated

Note. According to our calculation we would not be able to observe rainfall on Titan's surface within as less than two Titan days based on (Mitri et al. 2007). A list of the constants used in table calculations. Precipitation rate = 1.2 m/Tyr*. Evaporation rate = 30 m/Tyr*. Hydraulic conductivity K_{hy} = 3.14 m/Tyr, for high permeabilities of 1×10^{-14} m^2, low permeabilities of 1×10^{-10} m^2 ρ, the density of methane = 438.9 kg m^{-3} μ, the viscosity of methane = 2×10^{-4} Pa/s gravity of Titan, and g is 1.35 m s^{-2}.

5. Fog Scenario

Fogs are clouds in contact with the ground and are formed similarly to clouds—by condensation of warmer air to tiny water droplets. The particle size of fog particles might reflect brightly as was the case in the discovery of fogs at the south pole of Titan (Brown et al. 2009). Surface heating due to higher summer insolation at the poles might increase the humidity especially near the mare or liquid bodies on the north pole. This methane vapor in the air along with a plethora of available microscopic solid haze particles raining from the upper atmosphere might be conducive to form fogs.

The most probable fog candidate that aligns with the BEF scenario is "precipitation fog." As the extra methane vapor (from lakes and puddled rainfall) comes into contact with air that is already heavily saturated after the rainfall, it might cause the air to reach the dew point and form fog. However, whether the temperature difference (MacKenzie et al. 2019) between rain cloud height and warmer ground would be enough to saturate the air and form precipitation fogs has yet to be formally modeled.

Other probable scenarios could be "advection fog" or "valley fog." Advection fog occurs when warm air moves in over a cooler land surface. When warm ocean breezes in over cooler land especially along coastlines, the land cools the warm air below the dew point and advection fog forms. Part of the T106 feature that aligns with the Ligeia coastline could be advection fog (Figure 4).

Valley fog occurs when warm air passes over the upward slope of a cool mountain. As elevation increases, the mountain cools the air quickly, causing condensation and fog. Cook et al. (2015) classified regions around the Mare in the mountain chain category. Birch et al. (2017) classify regions around the north polar maria in their geological map as SAR-bright/dark dissected terrains, SAR-bright dissected uplands, and mountains. The topographic areas would form fog or low-level orographic clouds in the valleys between mountains or on the windward side of hills.

If BEFs behave the same as the WSW surface, they would be expected to occur in flat, open plains with minor changes in surface elevation while fogs are expected in low-elevation valleys between hills/mountains or the leeward side of the larger seas. According to our color images using the spectroscopic windows, if BEF features are fog, they are probably a few km or less off the surface or near-surface fogs. Depending on the humidity and temperature, fogs can form quickly and also disappear very quickly. Such "flash fogs" are transient in nature. The BEF features could as well be "flash fogs" owing to their ephemerality. However, their lifetimes can only be constrained provided the local climate conditions are known.

It is conceivable to have a scenario similar to ice crystals in Earth's atmosphere observed to produce broad specular reflections and thus appear more orange than purple in the BEF color scheme. On Titan, if aerosols (Tomasko et al. 2008) formed into little plates and settled in the atmosphere in parallel, we might get a reflection off the oriented plates. However, even these low-lying, ice-laden clouds should exhibit the high reflectance at 2.7 μm characteristic for clouds (which is not observed).

6. Result and Discussion

We report VIMS observations of BEFs over Titan's north pole. Their spectral signatures indicate they could be surface to near-surface features. Their proximity to direct specular reflections suggest that these features are broad specular reflections. These bright patches lie primarily over land surfaces but certain parts of their extend into fluid bodies highlighting the complex sea–land meteorological conditions at Titan's sea district (e.g., rain, fog, and convective clouds) as suggested by previous models (Tokano 2009).

The extension of regions of a BEF into fluid bodies is intriguing. We use a triple peak color scheme to untangle the regions of a BEF extending into liquid bodies. The liquid extensions of T119 and T123 flybys do show up in whitish hues indicating the non-surficial location of the features.

In the T106 flyby, the extension of a BEF into Ligeia Mare does not show up in whitish hues. This could either mean that we are looking at wavy liquid surfaces or a near-surface fog/cloud. A maria with surface roughness of 9°–15° could as well indicate active rainfall. Another possibility is we could just be observing a near-surface cloud that is obstructing the active rainfall happening at that very instant while Cassini VIMS is looking at the region. We could as well be seeing the falling drops themselves. The lower gravity and bigger raindrops (Lorenz 1993) fall slow compared to Earth and might outlast the cloud sometimes.

Figure 8 shows a time line of the observed BEF features. Highest precipitation in the warmer colors can be seen a little before 2015. Our time series suggests that the bright patches started in 2014 and picked up by 2016. The northern summer is probably inchoate compared to model predictions but definitely picked up, indicating dynamic progression of the atmosphere–surface interaction. The fact that our observations agree with the predictions is consistent with the idea that these phenomenon are meteorological. A comparison of Figure 1 of Turtle et al. (2018) indicates that ISS sees patchy clouds in 2014 and the cloud activity picks up by 2016 in ISS observations too.

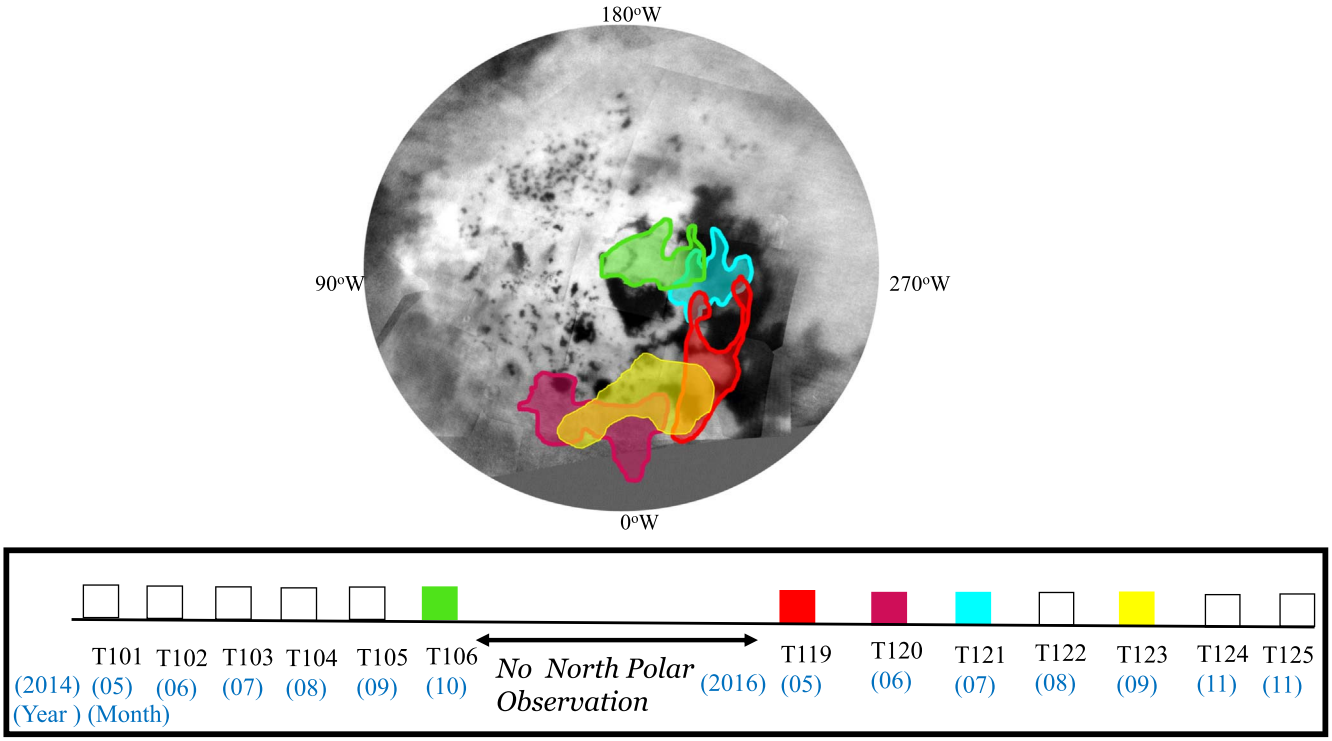

Figure 8. We show all the confirmed BEFs in the above polar plot of Titan. The time line below shows the appearance of the BEF on the north pole. The opaque boxes show a positive observation of the BEF while the white outlined boxes indicate unconfirmed observation. The numbers preceded by *T* are the flyby numbers. The numbers in blue state the month and year the observation was recorded in.

The geographical locations of the BEFs on the north pole are intriguing. The BEFs are confined to the polar latitudes north of Kraken's south shoreline (60°N), suggesting that the maria might be driving them. More usually than not the BEFs are located near the larger liquids on the north pole. This compels us to ask if the big seas and the humidity along with solar heating is driving these BEFs. This may also suggest that much of the methane humidity must originate from the maria. The solar heating of the north pole results in the warming of the cooler liquids that increase the humidity content near the liquid's surface. This increase in humidity might drive rainstorms or rainfall.

Titan's south polar summer deserves to be mentioned in our discussion as well. When Cassini arrived in Saturn's system in 2004 July, the summer had already started in the Southern Hemisphere and was in full swing. We did miss the beginning of the south polar summer. In contrast, we saw the beginning of the northern polar summer but the Solstice mission ended as the northern summer probably was in full swing.

In particular, we saw one large storm in the south polar summer (Turtle et al. 2011), while cloud activity was frequent (Turtle et al. 2018). In comparison, if the BEFs are rainfall events or even if they are precipitation fogs, we might have observed far more events on the north pole of Titan. The relative larger liquid cover of the north pole definitely affects the humidity levels that probably causes the larger cloud cover and more dynamic meteorology.

This documentation will help the design and execution of potential future Titan missions. Establishing the WSW effect technique would permit a future Titan orbiter (Coustenis et al. 2009; Mitri et al. 2014; Sotin et al. 2017), or Saturn orbiter with multiple Titan flybys, to map surface rainfall using broad specular reflections. Tighter constraints on rain would improve global understanding of methane transport. The knowledge of rainfall patterns might help design flight patterns of Titan aerial vehicles including balloons (Lorenz 2008a, 2008b; Dorrington 2011; Hall et al. 2011), airplanes (Barnes et al. 2012), and rotorcraft (Turtle et al. 2019).

The authors acknowledge support from the NASA/ESA Cassini Project and the VIMS team. R.D. acknowledges support from NPP (NASA Postdoctoral Program) and the Cassini team for all the years of profound work. We thank Dr. Faith Vilas for coordinating the reviews, Dr. Vincent Chevrier, and an anonymous reviewer for their careful reading and suggestions that improved our manuscript.

ORCID iDs

Rajani D. Dhingra https://orcid.org/0000-0002-3520-7381
Jason W. Barnes https://orcid.org/0000-0002-7755-3530
Jason M. Soderblom https://orcid.org/0000-0003-3715-6407
Stéphane Le Mouélic https://orcid.org/0000-0001-5260-1367

References

Barnes, J. W., Brown, R. H., Soderblom, L., et al. 2007a, Icar, 186, 242
Barnes, J. W., Buratti, B. J., Turtle, E. P., et al. 2013a, PlSci, 2, 1
Barnes, J. W., Clark, R. N., Sotin, C., et al. 2013b, ApJ, 777, 161
Barnes, J. W., Lemke, L., Foch, R., et al. 2012, ExA, 33, 55
Barnes, J. W., Radebaugh, J., Brown, R. H., et al. 2007b, JGRE, 112, E11006
Barnes, J. W., Sotin, C., Soderblom, J. M., et al. 2014, PlSci, 3, 3
Birch, S. P. D., Hayes, A. G., Dietrich, W. E., et al. 2017, Icar, 282, 214
Brown, M. E., Roberts, J. E., & Schaller, E. L. 2010, Icar, 205, 571
Brown, M. E., Smith, A. L., Chen, C., & Ádámkovics, M. 2009, ApJL, 706, L110

Cook, C., Barnes, J. W., Kattenhorn, S. A., et al. 2015, JGR, 120, 1220
Coustenis, A., Atreya, S., Balint, T., et al. 2009, ExA, 23, 893
Dhingra, R. D., Barnes, J. W., Brown, R. H., et al. 2019, GeoRL, 46, 1205
Dhingra, R. D., Barnes, J. W., Yanites, B. J., & Kirk, R. L. 2018, Icar, 299, 331
Dorrington, G. E. 2011, AdSpR, 47, 1
Griffith, C. A., Penteado, P., Rodriguez, S., et al. 2009, ApJL, 702, L105
Hall, J. L., Lunine, J., Sotin, C., et al. 2011, in Proc. Interplanetary Planetary Probe Workshop 8 (Houston, TX: NASA Johnson Space Center)
Hayes, A., Aharonson, O., Callahan, P., et al. 2008, GeoRL, 35, L9204
Heslar, M. F., Barnes, J. W., Seignovert, B., Dhingra, R. D., & Sotin, C. 2020, PSJ, submitted
Hofgartner, J. D., Hayes, A. G., Lunine, J. I., et al. 2016, Icar, 271, 338
Horvath, D. G., Andrews-Hanna, J. C., Newman, C. E., Mitchell, K. L., & Stiles, B. W. 2016, Icar, 277, 103
Kuiper, G. P. 1944, ApJ, 100, 378
le Mouélic, S., Rodriguez, S., Robidel, R., et al. 2018, Icar, 311, 371
Lora, J. M., & Mitchell, J. L. 2015, GeoRL, 42, 6213
Lorenz, R. D. 1993, P&SS, 41, 647
Lorenz, R. D. 2008a, JBIS, 61, 2
Lorenz, R. D. 2008b, AeJ, 112, 353
MacKenzie, S. M., Barnes, J. W., Hofgartner, J. D., et al. 2019, NatAs, 3, 506
MacKenzie, S. M., Lora, J. M., & Lorenz, R. D. 2019, JGRE, 124, 1728
McCord, T. B., Hansen, G. B., Buratti, B. J., et al. 2006, P&SS, 54, 1524
McCord, T. B., Hayne, P., Combe, J.-P., et al. 2008, Icar, 194, 212
Mitchell, J. L., & Lora, J. M. 2016, AREPS, 44, 353
Mitchell, J. L., Pierrehumbert, R. T., Frierson, D. M. W., & Caballero, R. 2006, PNAS, 103, 18421
Mitri, G., Coustenis, A., Fanchini, G., et al. 2014, P&SS, 104, 78
Mitri, G., Showman, A. P., Lunine, J. I., & Lorenz, R. D. 2007, Icar, 186, 385
Rannou, P., Montmessin, F., Hourdin, F., & Lebonnois, S. 2006, Sci, 311, 201
Rodriguez, S., le Mouélic, S., Rannou, P., et al. 2009, Natur, 459, 678
Rodriguez, S., le Mouélic, S., Rannou, P., et al. 2011, Icar, 216, 89
Soderblom, J. M., Barnes, J. W., Soderblom, L. A., et al. 2012, Icar, 220, 744
Soderblom, L. A., Tomasko, M. G., Archinal, B. A., et al. 2007, P&SS, 55, 2015
Solomonidou, A., Hirtzig, M., Coustenis, A., et al. 2014, JGRE, 119, 1729
Sotin, C., Hayes, A., Malaska, M., et al. 2017, in Proc. EGU General Assembly Conf. Abstracts (Göttingen: Copernicus), 10958
Sotin, C., Jaumann, R., Buratti, B. J., et al. 2005, Natur, 435, 786
Sprow, F., & Prausnitz, J. 1966, FaTr, 62, 1097
Steckloff, J., Soderblom, J. M., Farnsworth, K. K., et al. 2020, PSJ, 1, 26
Tokano, T. 2009, Icar, 204, 619
Tokano, T. 2011, Sci, 331, 1393
Tokano, T., & Neubauer, F. M. 2005, GeoRL, 32, L24203
Tomasko, M. G., Doose, L., Engel, S., et al. 2008, P&SS, 56, 669
Tomasko, M. G., & Smith, P. H. 1982, Icar, 51, 65
Turtle, E., Perry, J., Barbara, J., et al. 2018, GeoRL, 45, 5320
Turtle, E. P., Perry, J. E., Hayes, A. G., et al. 2011, Sci, 331, 1414
Turtle, E. P., Perry, J. E., McEwen, A. S., et al. 2009, GeoRL, 36, L2204
Turtle, E. P., Trainer, M. G., Barnes, J. W., et al. 2019, LPI, 50, 2888
Vargaftik, N., Volkov, B., & Voljak, L. 1983, JPCRD, 12, 817